Numerical simulation of coherent structure in two-dimensional compressible mixing layers*

FU Dexun (傅德薰) and MA Yanwen (马延文)

(Institute of Mechanics, Chinese Academy of Sciences, Beijing 100080, China)

Received April 5, 1996

Abstract The coherent structure in two-dimensional mixing layers is simulated numerically with the compressible Navier-Stokes equations. The Navier-Stokes equations are discretized with high-order accurate upwind compact schemes. The process of development of flow structure is presented: loss of stability, development of Kelvin-Helmholtz instability, rolling up and pairing. The time and space development of the plane mixing layer and influence of the compressibility are investigated.

Keywords: coherent structure, pairing, high-order accurate scheme.

Great achievement in study of incompressible turbulence with direct numerical simulation (DNS) has been reached. For typical flow models the computed results agree well with experiments, and some new mechanism has been observed with DNS. For many practical applications it is required to understand the compressible turbulent flow. Although the DNS for the compressible turbulence starts just in recent years, it develops very fast[1—3].

Recently people have paid more attention to the compressible mixing layers. One of the reasons is to understand the mechanism of reduction of the growth rate with increasing convective Mach number in order to increase the combustion rate of scramjet. On the other hand, the compressible mixing layer is a good model for study of compressible turbulence.

The unstationary flow field of compressible mixing layers with a range of scales and vortex-shock interaction is very complicated. To correctly simulate this kind of complex flow field the method must be highly accurate and can capture small structures of flow field. For the flow field with higher convective Mach number it is required that the method should have high resolution of the shock. The finite difference method is simple and easy manipulate. Besides, the method can be easily reconstructed to give high resolution of the shock.

In the present paper a high-order accurate scheme is used to simulate the compressible

* Project supported by the National Natural Science Foundation of China and the National Key Project for Basic Research.

mixing layer. The fifth-order accurate upwind compact difference operator developed by the authors is used to approximate the convection terms of the N-S equations, a sixth-order symmetrical compact difference operator is used to approximate the viscous terms, and a three-stage R-K method is used to advance in time. The present method has high accuracy and can capture flow structures with higher wave numbers. The upwind property of the scheme is useful for suppressing the oscillations with high frequency in the numerical solutions[4]. To better capture the shocks the scheme is modified with the method of diffusion analogy developed by the authors in ref. [5]. The process of losing stability, formation and development of the coherent structure are discussed. The obtained results for $M_c=0.2$ with three pairings agree well with the results in ref. [6] obtained with the spectral method. The influence of compressibility on the coherent structure and flow structure with vortex-shocklets are discussed.

1 Numerical method

1.1 Model equation and difference approximation

For simplicity consider the following model equation:

$$\frac{\partial u}{\partial t}+\frac{\partial f}{\partial x}=\mu\frac{\partial^2 u}{\partial x^2},\quad f=cu. \tag{1}$$

The corresponding semi-discrete approximation can be written as follows:

$$\frac{\partial u_j}{\partial t}+\frac{F_j}{\Delta x}=\mu\frac{S_j}{\Delta x^2}, \tag{2}$$

where $F_j/\Delta x$ is an approximation of $\partial f/\partial x$, and $S_j/\Delta x^2$ is an approximation of $\partial^2 u/\partial x^2$. For different approximations F_j and S_j have different expressions. The fifth-order accurate upwind compact approximation for the first derivative is as follows:

$$\frac{3}{5}F_j^+ + \frac{2}{5}F_{j-1}^+ = \delta_x^- \tilde{f}_j^+,\qquad c>0 \tag{3}$$

$$\frac{2}{5}F_{j+1}^- + \frac{3}{5}F_j^- = \delta_x^+ \tilde{f}_j^-,\qquad c<0 \tag{4}$$

$$\tilde{f}_j^{\pm}=[-f_{j\pm2}+11f_{j\pm1}+47f_j-3f_{j\mp1}]/60,$$

where $\delta_x^- f_j=f_j-f_{j-1}$, $\delta_x^+ f_j=f_{j+1}-f_j$. For the second derivative $\partial^2 u/\partial x^2$ the following sixth-order accurate symmetrical compact difference operator is used:

$$2S_{j-1}+11S_j+2S_{j+1}=12(u_{j-1}-2u_j+u_{j+1})+\frac{3}{4}(u_{j-2}-2u_j+u_{j+2}). \tag{5}$$

In solving eq. (2) in advance a three-stage R-K method is used. Rewrite (2) in the form

$$\frac{\partial u_j}{\partial t}=L(u_j).$$

The three-stage R-K method is expressed as follows:

$$u_j^{(1)} = u_j^{(n)} + \Delta t L(u_j), \tag{6a}$$

$$u_j^{(2)} = \frac{3}{4}u_j^{(n)} + \frac{1}{4}u_j^{(1)} + \frac{1}{4}\Delta t L(u_j^{(1)}), \tag{6b}$$

$$u_j^{n+1} = \frac{1}{3}u_j^{(n)} + \frac{2}{3}u_j^{(2)} + \frac{2}{3}\Delta t L(u_j^{(2)}). \tag{6c}$$

The method is explicit and has the third-order accuracy in time, and it requires less memory.

1.2 Governing equations and discretization

The two-dimensional compressible N-S equations for the perfect gas in the vector form can be written as

$$\frac{\partial U}{\partial t} + \frac{\partial f}{\partial x} + \frac{\partial g}{\partial y} = \frac{\partial}{\partial x} f_v + \frac{\partial}{\partial y} g_v, \tag{7}$$

$$U = [\rho,\ \rho u,\ \rho v,\ E]^{\mathrm{T}},$$

$$f = [\rho u,\ \rho u^2 + p,\ \rho uv,\ u(E+p)]^{\mathrm{T}},$$

$$g = [\rho v,\ \rho uv,\ \rho v^2 + p,\ v(E+p)]^{\mathrm{T}},$$

$$E = \left(C_v T + \frac{u^2+v^2}{2}\right).$$

The terms on the right-hand side of (7) are the viscous part of the N-S equations. ρ, p, u, v, and T stand for density, pressure, the velocity component in x and y directions, and the temperature, respectively. They are normalized by ρ_1, $\rho_1 u_1^2$, u_1, u_1, and T_1, respectively. The lower index 1 corresponds to the free flow conditions, and C_v is the specific heat. Rewrite eq. (7) in the form

$$\frac{\partial U}{\partial t} + \frac{\partial f^+}{\partial x} + \frac{\partial g^+}{\partial y} + \frac{\partial f^-}{\partial x} + \frac{\partial g^-}{\partial y} = \frac{\partial f_v}{\partial x} + \frac{\partial g_v}{\partial y}, \tag{8}$$

where

$$f^+ + f^- = f, \qquad f^\pm = A^\pm U,$$
$$g^+ + g^- = g, \qquad g^\pm = B^\pm U.$$

A and B are the Jacobian matrices:

$$A = \frac{\partial f}{\partial U}, \qquad B = \frac{\partial g}{\partial U},$$
$$A^\pm = S_a^{-1} \Lambda_a^\pm S_a, \qquad B^\pm = S_b^{-1} \Lambda_b^\pm S_b.$$

$\Lambda_a^\pm$ and $\Lambda_b^\pm$ are the diagonal matrices with elements $\lambda_k^\pm(A)$ and $\lambda_k^\pm(B)$, and

$$\lambda^\pm = \frac{1}{2}(\lambda \pm |\lambda|),$$

where $\lambda_k(A)$ and $\lambda_k(B)$ are the eigenvalues of the matrices A and B, respectively.

Now we briefly describe the discretization method for the N-S equations. The terms $\partial f^+/\partial x$ and $\partial g^+/\partial y$ are approximated with the difference operator of type (3), and $\partial f^-/\partial x$ and $\partial g^-/\partial y$ are approximated with difference operator type (4). The terms in the viscous part of the equations have form $\partial(K\partial g/\partial x_j)/\partial x_i$ ($i=1, 2$; $j=1, 2$; $x_1=x$, $x_2=y$; and $g=u$, v and T). This kind of terms can be approximated with two times application of the difference operator approximating the first derivative. For example, consider $\frac{\partial}{\partial x}\left(\mu\frac{\partial u}{\partial x}\right)$. Denote by $F_j/\Delta x$ the approximation of $\partial u/\partial x$, and by $G_j/\Delta x$ the approximation of the sixth-order accurate symmetrical compact operator in ref. [3] is used to approximate the first derivative as follows:

$$\frac{1}{5}F_{j+1}+\frac{3}{5}F_j+\frac{1}{5}F_{j-1}=\frac{14}{15}\delta_x^0 u_j+\frac{1}{30}\delta_x^0(u_{j+1}-u_{j-1}), \tag{9a}$$

$$\frac{1}{5}G_{j+1}+\frac{3}{5}G_j+\frac{1}{5}G_{j-1}=\frac{14}{15}\delta_x^0(\mu F_j)+\frac{1}{30}\delta_x^0[(\mu F)_{j+1}-(\mu F)_{j-1}], \tag{9b}$$

$$G_j=(\mu F)_j/\Delta x, \quad G_j/\Delta x \cong \frac{\partial}{\partial x}\left(\mu\frac{\partial u}{\partial x}\right), \tag{9c}$$

where $\delta_x^0 u_j=(u_{j+1}-u_{j-1})/2$. To solve the obtained semi-discrete equations approximating the N-S equations the R-K method (6) is used in advance. The obtained discretized equations have the third-order accuracy in time.

2 Numerical simulation of the compressible mixing layers

Suppose at the very beginning we have a thin membrane separating two flows with equal velocity but in opposite directions. Suddenly the membrane is broken, and free shear flow is formed. This flow is unstable, and soon is rolling up and pairing. This process of flow development is simulated with the above presented method.

2.1 Initial and boundary conditions

The initial conditions consist of a parallel mean flow with a hyperbolic tangent profile plus perturbation of the velocity components. The mean profile of the velocity is specified by the following relations:

$$\begin{aligned}&\bar{u}=A[B+\tanh(\beta y)], \qquad \beta>0,\\ &\bar{v}=0,\\ &A=(u_1-u_2)/2, \qquad B=(u_1+u_2)/2,\end{aligned} \tag{10}$$

where u_1 and u_2 correspond to the upper and lower undisturbed flow respectively

Initial perturbations of the velocity are described by the following expressions:

$$u' = \sum_{1\leqslant j\leqslant 4} \varepsilon_j \{\varphi'_{\alpha_j,r}(y)\cos(\alpha_j x) - \varphi'_{\alpha_j,i}(y)\sin(\alpha_j x)\},$$

$$v' = \sum_{1\leqslant j\leqslant 4} \varepsilon_j \alpha_j \{\varphi_{\alpha_j,r}(y)\sin(\alpha_j x) + \varphi_{\alpha_j,i}(y)\cos(\alpha_j x)\}, \tag{11}$$

where the wave number $\alpha_1 = 0.444\,6$ corresponds to the most unstable mode obtained from linear inviscid analysis given in ref. [7]. $\varphi_{\alpha_1,r}$ and $\varphi_{\alpha_1,i}$ are the real and imaginary part of the corresponding eigenfunction for the streamfunction, $\varphi'_{\alpha_1,r}$ and $\varphi'_{\alpha_1,i}$ are derivatives of $\varphi_{\alpha_1,r}$ and $\varphi_{\alpha_1,i}$ with respect to y; $\varphi_{\alpha_2,r}$ and $\varphi_{\alpha_2,i}$ are the real and imaginary part of the eigenfunction corresponding to the wave number α_2, and $\varphi_{\alpha_2,r}$, $\varphi_{\alpha_2,i}$ and $\varphi'_{\alpha_2,r}$, $\varphi'_{\alpha_2,i}$ are corresponding eigenfunctions and their derivatives. The initial non-dimensional pressure is equal to $1/(\gamma M_\infty^2)$ (in the present paper $M_c = M_\infty$). The initial temperature is obtained from the Busemann-Crocco relation $T_1 = T_2 = \left[1 + \frac{\gamma-1}{2} M_\infty^2 (1-\bar{u}^2)\right]$. The initial density is obtained from the state equation with given p and T. The convective Mach number is defined as in ref. [8]: $M_c = (u_1 - u_2)/(c_1 + c_2)$, where c is the sound speed, indices 1 and 2 correspond to the upper and lower flow parameter respectively. The initial thickness is taken as the characteristic length. In the computation $u_1 = -u_2 = 1$, $\beta = 1$, $\varepsilon_1 = \varepsilon_2 = \varepsilon_3 = \varepsilon_4 = 0.05$, $\alpha_1 = 0.444\,6$, $\alpha_2 = \alpha_1/2$, $\alpha_3 = \alpha_1/4$, $\alpha_4 = \alpha_1/8$, $Re = 400$, are used. For the case of three pairings the computational region is defined as

$$0 \leqslant x \leqslant 16\pi/\alpha_1, \quad -12\pi/\alpha_1 \leqslant y \leqslant 12\pi/\alpha_1.$$

The undisturbed upper and lower flow parameters are taken as the boundary conditions at the corresponding boundaries. The periodic boundary conditions are used in the x direction.

2.2 Computed results

In order to test the developed method the cases as in ref. [9] with the same conditions for $M_c = 0.4$ and 0.8 were computed. The variation of the vorticity thickness with time is given in fig. 1. The solid line is for the case $M_\infty = 0.4$, and the dash line is for the case $M_\infty = 0.8$. In the present computation $IN \times JN = 76 \times 76$ mesh grid points are used. From the figures it can be seen that the growth rate of the vorticity thickness is decreased with increasing

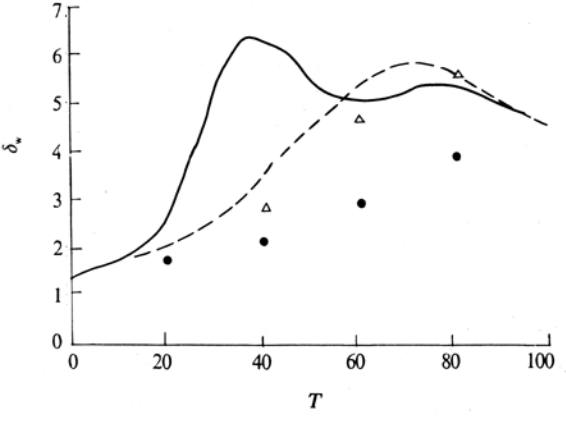

Fig. 1. Variation of vorticity thickness versus time.

convective Mach number. In this figure are also given the results computed in ref. [4] with TVD schemes for the case of $M_\infty=0.8$. The circles are for the case of 75×75, and the triangles are for the case of 150×150. It can be seen that the method in the present paper gives better results with less grid points.

In the following computation the initial conditions consist of a parallel mean flow plus perturbation of the velocity components. The perturbed velocity components consist of a basic harmonic plus three subharmonics. This kind of initial conditions lead to three pairings. For the case of $M_c=0.2$ the system of mesh grid points is $IN\times JN=200\times200$, and for the case of $M_c=0.8$, $IN\times JN=502\times156$. The vorticity contours at different characteristic time for the case of $M_c=0.2$ are given in fig. 2. The characteristic times are defined as: T_{pn}, the nth pairing time of the rollers, T_{sn}, the time at which the vorticity from the spiral arms back into the braid region. The computed results for the case of $M_c=0.2$ show that the free shear flow loses its stability at first, and then the Kelvin-Helmholtz unstable waves develop. In some interval the perturbations grow exponentially. Under action of the perturbation with the basic mode the vorticity distributed almost uniformly in the streamwise direction at the beginning starts to be redistributed in the streamwise direction, and eight orderly K-H rollers are formed soon. After a while the effect of nonlinearity increases, and the growth of the perturbation with the first subharmonic becomes obvious. This phenomenon leads to the first vortex pairing (see fig. 2 at $T=40.00$). Pairs of well-developed rollers come together, corotate and eventually amalgamate. The number of rollers is reduced by half from eight to four. In the process of pairing the contents of every other braided region are absorbed into the new paired roller. The surviving braided region continues to be depleted of spanwise vorticity as all the vortical fluid is drawn into the paired roller. As the cores of the original spanwise rollers merge into a new core, spiral arm of weaker spanwise vorticity is ejected away from the paired eddy due to energy

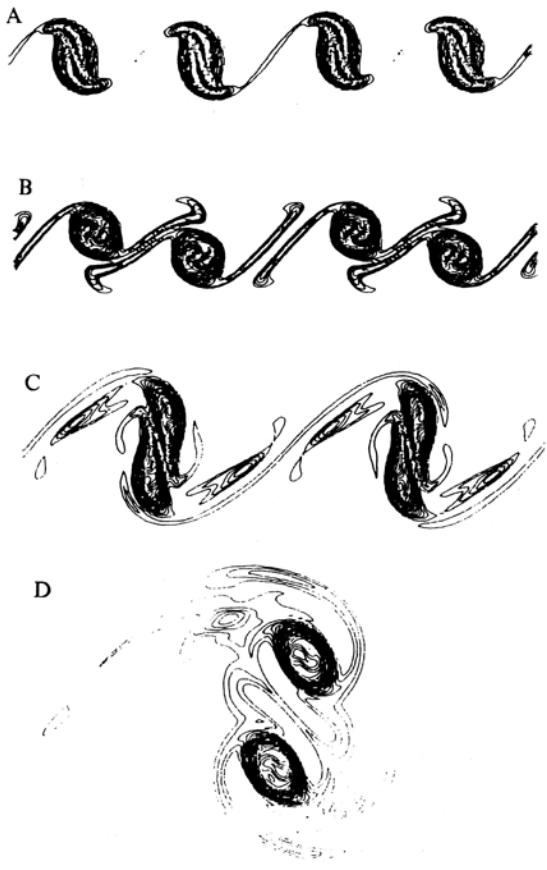

Fig. 2. Vorticity contours for $M_c=0.2$, A: $T=40.00(T_{1p}=40.33)$, B: T=65.33 ($T_{1s}=65.33$), C: $T=93.33$ ($T_{2p}=92.33$), D: $T=213.33$ ($T_{3p}=215.63$).

conservation[6] (see fig. 2 at $T=65.33$). This process repeats itself during each pairing. In fig. 3 are given the variations of δ_m and $-\omega_b$ with time t. δ_m is the momentum thickness, and ω_b is the minimum of the spanwise vorticity at the point $x=0$ in the present computation.

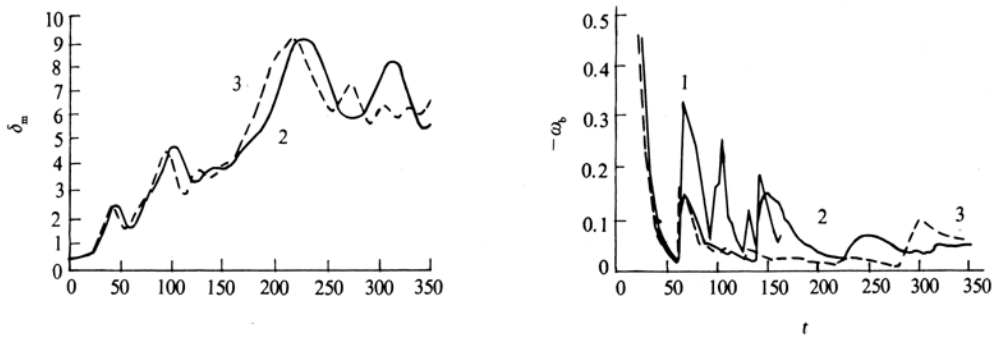

Fig. 3. Variation of δ_m and $-\omega_b$ versus time. 1, $M_c=0.4$, one pairing; 2, $M_c=0.4$, three pairings; 3, $M_c=0.2$, three pairings.

From the figure it can be seen that $-\omega_b$ is small just before each pairing. This is because the vorticity in the braid region is absorbed into the new paired roller. After that we see suddenly the increase of $-\omega_b$ in fig. 3. This is because of vorticity ejection away from the paired eddy. After multiple pairings we can also see increase of the vorticity in the braid region. This vorticity in the braid region is convected during the time of oversaturation. From fig. 3 it can be seen at the pairing time T_{pn} that the momentum thickness reaches its maximum. After each pairing the streamwise scale and the thickness of the mixing layer are two times enlarged but the velocity scale is not changed, so the time scale is two times enlarged too. This can be seen from fig. 3 and table 1. In table 1 are given the characteristic times computed in the present paper. In this table are also given the results computed in ref. [6] with the spectral method for the incompressible mixing layer for comparison. It can be seen that the agreement is good for the case $M_c=0.2$. The flow structures computed in the present paper for the case of $M_c=0.2$ agree well with the incompressible results in ref. [6]. This means that the flow structures are almost incompressible, and the method developed in the present paper is efficient for computing the compressible mixing layers.

Table 1 Characteristic time[a)]

Characteristic time	2-D Incompressible	2-D $M_\infty=0.2$, $Re=400$ three pairings	3-D Incompressible	3-D $M_\infty=0.2$, $Re=400$ one pairing
T_{p1}	21.5	20.17	21.5	21.6
T_{p2}	47.0	46.17		
T_{p3}	103.7	107.81		
T_{s1}	32.0	32.66		
T_{s2}	66.7	66.33		

a) For comparison the time scale is changed according to reference [6].

2.3 Effect of compressibility

Experiments show that the growth rate decreases with increasing convective Mach number. The same trend is obtained from the present computation (see fig. 1). In ref. [1] the flow mechanism for the compressible mixing layers was analyzed mainly for the range of linear growth. In the present paper the flow mechanism is discussed on the basis of numerical simulation of three pairings. The coherent structure in the compressible mixing layers is controlled by wave-eddy interaction. It is known that there are longitudinal and transverse (or eddy) waves in the compressible flow. The longitudinal waves are induced by the compression and expansion. The examples are the Mach waves and shock waves. The transverse or eddy waves are produced due to the shear stress. The example is the Kelvin-Helmholtz waves (or K-H waves). Development of eddy waves leads to the formation of the longitudinal waves. The interaction between the transverse and longitudinal waves defines the coherent structure in the compressible mixing layers.

For the incompressible mixing layers the vorticity production and its redistribution are caused by the instability of the transverse waves. Increase of the instability leads to the formation of the vortex roller. The vorticities are carried from the stagnation points between the rollers into the vortex core, and the thickness of the mixing layers increases. For the compressible mixing layers, except the mechanism of vorticity rolling up and pairing as for the incompressible mixing layers the flow around the vortex is expanded and accelerated leaving from the stagnation point, and then compressed and decelerated towards the other stagnation point. This process leads to the production of the longitudinal waves, the expansion and the compression waves. Such expansion and compression make the vorticity reduce near the vortex center and increase near the stagnation points. This is opposite to the redistribution arising from the instability of the transverse waves[1]. Thus the compressibility leads to the decrease of the growth rate of the compressible mixing layers. It can be seen from fig. 3 that the growth rate in the range of linear theory for $M_c=0.2$ and 0.4 is almost the same (agreeing with the results in ref. [1]), but the vortex pairing is delayed (see table 1) because of the influence of the longitudinal waves which makes the vorticity distribution more uniform in the streamwise direction. As was shown in ref. [6] for the incompressible mixing layer the only mechanism for spreading out the vorticity is viscous diffusion, and since the Reynolds number doubles with each pairing, diffusion cannot keep pace with the pairings. The resulting paired rollers have high vorticity concentrated in a relatively small area (see fig. 2, the flow structure for $M_c=0.2$ is much similar to the incompressible). Comparing fig. 4 with fig. 2 we see that the flow expansion and compression prevent the vorticity concentration, and make the rollers spread. The compressibility effect increases with increasing convective Mach number. The effect of two kinds of waves becomes comparable, and the growth rate of the mixing layer decreases obviously. The vorticity and density contours at three pairing times for $M_c=0.8$ are given in fig. 4.

The process of expansion and compression is very clear. During the process of first pairing the flow around the vortex is expanded and accerelated to locally supersonic speed and, in order to reach the stagnation point between the vortices, it has to be compressed. The shock is formed due to converging of the compression waves and is extended to the field away from the central line. The flow becomes subsonic across the shock, and enters the braid region. The flow is futher compressed to the stagnation point. Then we can see eddy-shocklets (see figs. 4, 5 at $T=64$).

During the process of pairing the shape and the strength of the shocks are changed. The braided region between two weak shocks becomes smaller, and it becomes larger between two stronger shocks. This event creates conditions for the next pairing. After that the shocks change their shape and strength continuously with closing of the neighbour rollers. From fig. 4 it can be seen that the vortex structure for the convective Mach number $M_c=0.8$ still is large. From the computed results we see that after each pairing the number of rollers is reduced by half, the vorticity thickness and the length between two rollers are two times enlarged, and the number of the shocks is reduced by half too. All these events show that the coherent structure of the compressible mixing layers is defined by interaction between the waves and eddies.

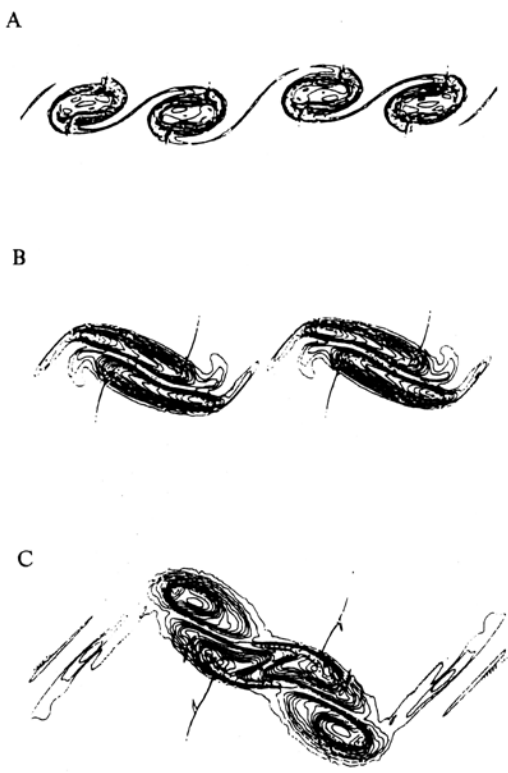

Fig. 4. Vorticity contours for $M_c=0.8$ at different times. A, T=64.00; B, $T=96.00$; C, $T=223.88$.

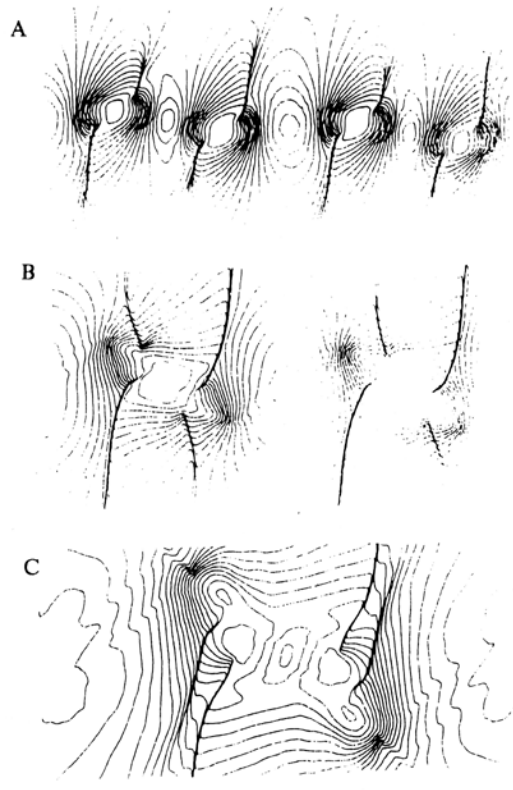

Fig. 5. Density contours for $M_c=0.8$ at different times. A, $T=64.00$; B, $T=96.00$; C, $T=223.88$.

Acknowledgement The authors are very grateful to Prof. Zhou Heng for useful discussion.

References

1 Lele, S. K., Direct numerical simulation of compressible free shear flow, *AIAA Paper*, 1989, 89—0374.
2 Rai, M. M., Moin, P., Direct numerical simulation of transition and turbulence in a spatially evolving boundary layer, *J. of Comput. Phys.*, 1993, 109: 169.
3 Lee, S., Lele, S. K., Moin, P., Eddy shocklets in decaying compressible turbulence, *J. Phys. of Fluids*, Ser. A, 1991, 3(4): 657.
4 Fu Dexun, Ma Yanwen, Numerical simulation of physical problems and high-order accurate difference schemes, *Chinese J. of Comput. Phys.* (in Chinese), 1992, 9(4): 501.
5 Ma Yanwen, Fu Dexun, Diffusion analogy and shock capturing for solving aerodynamic equations, *Science in China*, Ser. A, 1992, 35(9): 1090.
6 Moser, R. D., Rogers, M. M., The three-dimensional evolution of a plane mixing layer: pairing and transition to turbulence, *J. Fluid Mech.*, 1993, 247: 275.
7 Michalke, A., On the inviscid instability of the hyperbolic-tangent velocity profile, *J. Fluid Mech.*, 1964, 19: 543.
8 Papamoschou, D., Roshko, A., The compressible turbulent mixing layer: An experimental study, *J. Fluid Mech.*, 1988, 197: 453.
9 Sandham, N. D., Yee, H. C., A numerical study of a class of TVD schemes for compressible mixing layers, *NASA-TM*-102194, A-89139, 1989.